Journal of Materials Chemistry A

Accepted Manuscript

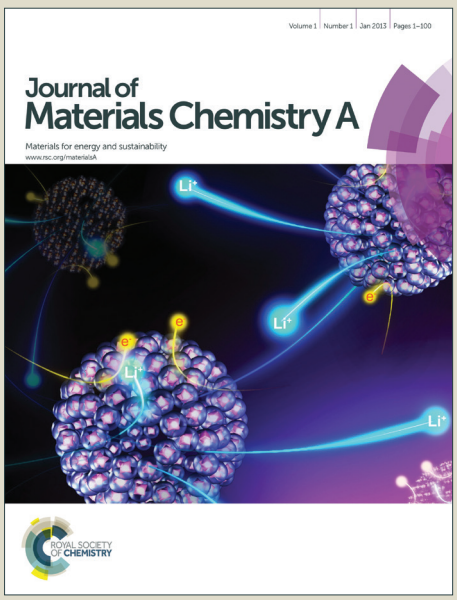

ROYAL SOCIETY OF CHEMISTRY

www.rsc.org/materialsA

Amorphous $Na_2Si_2O_5$ as a Fast Na^+ Conductor: an *Ab-initio* Molecular Dynamics Simulation

Xueling Lei [a, b], Youngseok Jee [b] and Kevin Huang [b,*]

[a] Department of Physics, Jiangxi Normal University, Nanchang, Jiangxi 330022, China

[b] Department of Mechanical Engineering, University of South Carolina, Columbia, SC 29208, USA

Abstract

The present work uses *ab-initio* molecular dynamics (AIMD) methodology to simulate ionic transport in the amorphous and crystalline $Na_2Si_2O_5$ from 573 to 973 K. The results suggest that the amorphous $Na_2Si_2O_5$ is primarily a Na^+ conductor with negligible O^{2-} and Si^{4+} contributions to the ionic conduction, whereas the crystalline $Na_2Si_2O_5$ is virtually an electrical insulator. The favorable pathway for Na^+ transport in the amorphous Na_2Si_2O is along the two-dimensional channels formed by the SiO_4 tetrahedra layers. The disrupted Na-O coulombic attraction by the long-range disorder in the amorphous $Na_2Si_2O_5$ contributes to the enhanced Na^+ conduction.

Keywords: sodium ion conductor; amorphous; crystalline; energy barrier; sodium ion transport

* Corresponding author: huang46@cec.sc.edu.

I. Introduction

The pursuit of high-conductivity solid electrolyte materials has long been of interest to solid-state chemists/electrochemists because of the significance it can bring to advance the development of high-power, high-capacity and efficient electrochemical cells such as fuel cells and batteries for a variety of energy applications [1-3]. Recently, a new family of oxides bearing a generic formula of $Sr_{1-x}A_xSiO_{3-0.5x}$ (A=Na, K) has been reported and immediately garnered much attention due to its high ionic conductivity, *e.g.* 0.01 S/cm at 500^oC [4-7]. The report quickly drew criticisms from groups that conducted follow up research [8-13]. These studies presented compelling evidence that the material was virtually a two-phase mixture, for example, consisting of a $SrSiO_3$ phase and amorphous $Na_2Si_2O_5$ phase for the $Sr_{1-x}Na_xSiO_{3-0.5x}$ system [9-13]. The $SrSiO_3$ phase was an electrical insulator while the amorphous $Na_2Si_2O_5$ phase was a good ionic conductor. The high conductivity observed in $Sr_{1-x}Na_xSiO_{3-0.5x}$ essentially stemmed from the amorphous $Na_2Si_2O_5$ phase. However, the nature of ionic conduction in the amorphous $Na_2Si_2O_5$, *e.g.* Na^+ *vs* O^{2-}, remained ambiguous until now.

Early MD simulations on the ionic diffusion in a glassy $Na_2Si_2O_5$ have focused mainly in the higher temperature range [14-16]. For example, Smith *et al.* simulated the ionic transport for sodium disilicate glass in a temperature range of 1000 - 2000 K in one study [14] and for alkali-metal disilicate glasses at 1400 K in another study [16]. No work has been reported so far on the solid-state amorphous $Na_2Si_2O_5$ in a lower temperature range such as below 1000 K. In the present study, we aim to elucidate the ionic conduction mechanisms in the amorphous $Na_2Si_2O_5$ from a computational perspective, *i.e.* applying *Ab-initio* Molecular Dynamics

(AIMD) methodology to simulate ionic transport in a solid-state amorphous $Na_2Si_2O_5$ in a temperature range of 573 - 973 K, a preferred operating temperature range for reduced-temperature solid oxide fuel cells (SOFCs). The work is of great importance not only to the understanding of ionic conduction mechanisms in solid-state $Sr_{1-x}A_xSiO_{3-0.5x}$, but also identification of new solid-state ionic conductors in the future.

II. The simulation method

The first-principles calculations in this study were performed using the projector augmented wave (PAW) method [17-18] included in a commercial VASP code [19-20]. The Na $2p^6 3s^1$, O $2s^2 2p^4$, and Si $3s^2 3p^2$ electrons were considered as valence electrons. The general gradient approximation (GGA) parameterized by Perdew Burke Ernzerhof (PBE) was used for the exchange–correlation terms [21], and wave functions were expanded by plane waves with a cut-off energy of 500 eV. The atomic positions were optimized until residual ionic forces became less than 0.02 eV $Å^{-1}$.

For the *ab-initio* Molecular Dynamics (AIMD) simulations of ionic transport, the canonical ensemble (NVT) was employed. A Verlet algorithm was integrated with Newton's equations of motion at a time step of 2 fs for a total simulation time of 40 ps, *i.e.*, 20,000 steps. The frequency of the temperature oscillations was controlled by the Nosé mass during the simulations. A supercell 1×2×2 unit cells (144 atoms) was used with a *k*-point sampling at the Γ-point.

To create an amorphous structure, the supercell was first melted by virtually heating it to

5,000 K within the NVT ensemble. Then, a melt configuration was randomly chosen to test the optimal lattice constant while considering the change in system volume induced by the phase transition. Finally, the melt configuration was subjected to a cooling process at a rate of 2.67×10^{13} K/s to obtain an amorphous structure.

For comparison, Na-ion transport in the crystalline $Na_2Si_2O_5$ was also simulated, in which a supercell of 1×2×2 (144 atoms) with a 2×2×1 *k*-point grid sampling was used together with the nudged elastic band (NEB) to seek for the saddle points and minimum energy pathways [22-23].

III. **Results and Discussion**

3.1. Na^+ diffusion in the amorphous $Na_2Si_2O_5$

3.1.1 Structure and electronic properties of a $Na_2Si_2O_5$ crystal

The $Na_2Si_2O_5$ has a triclinic structure (SG: *P1*), the unit cell of which is depicted in Fig.1 (a) as SiO_4 layers with Na^+ residing in between the corner-shared SiO_4 layers for charge compensation. From the calculated density of states (DOS), Fig.1 (b), the band gap of the crystalline $Na_2Si_2O_5$ is 4.22 eV, which essentially indicates that it is an electrical insulator. The calculated lattice constants and structural parameters listed in Table 1 agree well with the experimental data [24], validating the computational method and parameters used.

3.1.2 Testing lattice constants for the amorphous $Na_2Si_2O_5$

To perform a rational AIMD simulation under the required constant volume condition in the

VASP code, the system volume change induced by the phase-transition needs to be determined so that a proper volume can be applied to the calculation. To do so, the optimal lattice constants for the amorphous $Na_2Si_2O_5$ structure need to be obtained first. As described in Section II, a melt configuration was randomly chosen and relaxed for 40 ps at each volume. Fig.2 shows the average free energy *vs* lattice constant scale factor. It is evident that the influence of volume on the free energy is relatively small. The best lattice constant scale factor was found to be 1.015, implying a 4.5% volume expansion after melting. In the following AIMD simulations, the lattice parameters of all the structures were multiplied by 1.015, aiming to more accurately calculate potential energy and free energy.

3.1.3 Structure and radial distribution function (g(r))

The AIMD simulations within the NVT ensemble were conducted in a temperature range of 573 - 973 K. The amorphous structures were obtained by the methods descried in Section II. As an example, Fig.3 (a) and (b) compare the amorphous structure simulated at 973 K with the crystalline structure. To extract the structural information, the present study calculated radial distribution function (RDF), $g(r)$, for the total and partial properties. Fig.3 (c) and (d) show the total g(r) as a function of radius (r) for the crystalline and amorphous $Na_2Si_2O_5$, respectively. For the crystalline $Na_2Si_2O_5$, crystallographic ordering is clearly seen at both the long- and short-range scale, whereas only a short-range ordering is observed for the amorphous $Na_2Si_2O_5$. In specific, there are two sharp peaks at a radius of 1.65 and 2.65 Å for the amorphous $Na_2Si_2O_5$, corresponding to the nearest Si-O and O-O separations, respectively, and a shoulder at 2.35 Å associated with the nearest Na-O separation. These RDF distributions are in good agreement with those obtained from neutron diffraction on the

same $Na_2Si_2O_5$ glass [25]; the latter study revealed two sharp peaks at a radius of 1.7 and 2.6 Å, and a broad peak at a radius of 2.4 Å associated with the nearest Na-O separation.

The partial RDF for the amorphous $Na_2Si_2O_5$ simulated at 973 K is further plotted in Fig.4; the results for other temperatures are similar. From the peak positions in a partial RDF, the peaks appeared in the total RDF shown in Fig.3 (d) can be further interpreted. For example, the strong first peak at a radius of 1.65 Å in the partial Si-O RDF is responsible for the first peak in the total RDF. Integration of the partial Si-O RDF indicates 3.92 O atoms surrounding each Si atom, indicating SiO_4 tetrahedral units present in the amorphous $Na_2Si_2O_5$. The first peak at a radius of 2.35 Å in the partial Na-O RDF is weak in the simulated total RDF. The strong first peak in the partial O-O RDF agrees well with the prominent peak in the total RDF at a radius of 2.65 Å, which reflects the O-O separation in a SiO_4 tetrahedron. The second strong peak in the partial O-O RDF is at a radius of 4.95 Å. A simple estimate from the atomic structure suggests that this peak is associated with the O-O separation from one tetrahedron to the other. The first peaks in the partial Si-Si and Na-Si RDF at radii of 3.05 and 3.15 Å, respectively, appear to be responsible for the weak features in the same region of the total RDF. Finally, it is noted that the first peak in the partial Na-Na RDF at a radius of 3.25 Å is almost invisible in the total RDF, implying a fast Na^+ transport.

3.1.4 Mean-squared displacement, diffusion coefficient, and conductivity

From a statistical physics perspective, the random diffusion of an ionic species in a material can be described by the mean square displacement (MSD). It is well known that the plots of MSDs for all ions feature plateaus independent of time for a poor conductor, whereas they

exhibit monotonic increase with time for a good conductor. The MSD of ions in a simulation can be computed by:

$$\mathrm{MSD} = <\delta r^2> = <[r_m(t+t_0) - r_m(t_0)]^2> = \frac{1}{N}\sum_m [r_m(t+t_0) - r_m(t_0)]^2 \quad (1)$$

where N is the total number of ions, $r_m(t+t_0)$ and $r_m(t_0)$ are the displacements of m^{th} ion at $t+t_0$ and t_0 time, respectively. The chevrons represent ensemble average. In the present work, a total of three MD simulations were performed for the same structure at each temperature, aiming to obtain an averaged MSD for accuracy. Fig.5 shows the average MSD calculated for Na^+, O^{2-}, and Si^{4+} in the amorphous $Na_2Si_2O_5$ from 573 to 973 K. Evidently, the MSD of Na^+ increases linearly with time, indicating a fast Na^+ transport. On the contrary, the MSDs of O^{2-} and Si^{4+} are almost parallel to the time axis, implying immobile O^{2-} and Si^{4+}. The distinct feature in Fig.5 strongly suggests that Na^+ is the predominant charge carrier in the amorphous $Na_2Si_2O_5$.

The average self-diffusion coefficient (D) of ions can be determined from the slope of the average MSD plots:

$$D = \lim_{t\to\infty} \frac{<\delta r^2>}{6t} \quad (2)$$

However, one should keep in mind that D herein is not a chemical diffusion coefficient used in the Fick's equation describing diffusion flux of species under a chemical concentration gradient. Instead, it is a self-diffusion coefficient describing the ability to diffuse under no concentration gradient. The correlation between the self-diffusion coefficient D and direct current ionic conductivity σ is given by the Nernst–Einstein relation:

$$\sigma_{dc} = \frac{N_{ion} q^2 D}{H_R k_B T} \quad (3)$$

here N_{ion} and q are the number density and charge of the mobile ion, respectively; k_B is the Boltzmann's constant; T is the absolute temperature; H_R is the Haven ratio between the tracer diffusivity D* and charge diffusivity D_σ: $H_R = D^* / D_\sigma$, describing the correlations between the hopping movements of mobile ions [26]. It is common to assume that the self-diffusion coefficient D is equal to the tracer diffusivity D* because of the nature that they both describe the ability of an ion to diffuse under no concentration gradient. It was also shown in Ref [27] that the charge diffusivity of Na^+ was very close to its tracer diffusivity for a soda-lime silicate glass. Therefore, H_R was taken as 1 in the present study.

Table 2 summarizes the calculated average D values for Na^+, O^{2-} and Si^{4+} at each temperature. Clearly, the D of Na^+ is about two orders of magnitude higher than those of O^{2-} and Si^{4+}, confirming that the amorphous $Na_2Si_2O_5$ is a Na^+ but not an O^{2-} or Si^{4+} conductor. Compared to Na^+-β″-Al_2O_3, a well-known Na^+-conductor, D_{Na} is roughly one-order of magnitude lower [28]. It is also interesting to note that D_{Na} is approximately two-to-three orders of magnitude higher than that of the glass $Na_2O{\cdot}2SiO_2$ at $T<T_g$, (T_g=465°C here is the glass transition temperature), whereas it is in good agreement with that of the glass $Na_2O{\cdot}2SiO_2$ at $T>T_g$, [29]. It is worth mentioning that the low D_O and D_{Si} values are well within the uncertainty of the method considering the limited total run time (40ps) for the MD simulation and the size of cell (144 atoms) employed. With a longer MD time and larger cell size, the accuracy of the simulation can be further improved.

The cause for the low O^{2-} diffusivity is the strong bonding between O and Si in the stable

SiO_4 tetrahedra, which is consistent with the analysis of partial RDFs. It is also noted that, while D_{Na} increases in general with temperature, a peculiar sudden increase is observed at 773 K, implying a possible phase transition occurred at this temperature. Although the precise reason for the discontinuity is not clear at the present time, 773K does coincide with the glass-to-ceramic transition temperature identified by DSC and high-temperature XRD [30].

Table 2 also compares the measured conductivity of amorphous $Na_2Si_2O_5$ with the simulated one at different temperatures. In general, they are in the same 10^{-3}~10^{-2} S/cm order of magnitude. Other than the likely small compositional difference between the theoretical $Na_2Si_2O_5$ and experimental sample that may contain partial crystalline phase formed during synthesis, the lower experimental σ could also be related to a continuous crystallization of the amorphous $Na_2Si_2O_5$ during the conductivity measurement; the latter has been thoroughly discussed in our recent publication [30].

Fig.6 shows the Arrhenius plot of D_{Na}; a kink is clearly visible at 723-773K. From the slope of the straight-line, the activation energies (E_a) are calculated to be 0.17 and 0.30 eV for the 573-723K and 773-973K segments, respectively. While these activation energies are somewhat lower than the previously calculated value of 0.56 eV [14] and experimental result of 0.69 eV for the $Na_2Si_2O_5$ glass [31], the E_a=0.30 eV for 773-973K segment is in good agreement with 0.222 – 0.276 eV within 100-370°C and 0.15 – 0.19 eV at >370°C reported for Na-β″-Al_2O_3 [28], but lower than 0.60 eV of a NASICON-type Na^+-conductor [32]. Moreover, the calculated E_a is very close to 0.32 eV observed for the $Sr_{3-3x}Na_{3x}Si_3O_{9-1.5x}$ (x=0.45) (SNS) compound [7]. Compared to other known oxide-ion conductors, *viz.* 0.53 eV and 0.64 eV for Sr-doped $La_{10}Si_6O_{27}$ [33] and Gd-doped CeO_2 electrolytes, respectively, the calculated E_a shows

lower value [34]. The corresponding pre-exponential factors for the Na^+ diffusion are 0.3×10^{-4} and 2.4×10^{-4} cm^2/s, respectively, which is on the same order of magnitude as 2.6×10^{-4} cm^2/s obtained from the previous MD simulation [14]. The differences observed between this study and a previous one are probably attributed to the different computational method employed and temperature range studied; the latter simulation used the empirical pair-potential method over a temperature range of 1000-2000 K.

3.1.5 The diffusion pathway of Na^+

The knowledge of Na^+ diffusion pathways is critically important to the understanding of ionic transport mechanisms in the amorphous $Na_2Si_2O_5$. Fig.7 (a)-(e) show a series of the snapshots of Na^+ positions at 873K in a time interval of 10 ps for a total of 40 ps; the green ball represents one Na^+ in motion. Comparison of Na^+ positions at each snapshot indicates a fast Na^+ diffusion as evidenced by the appreciable positional change of each snapshot. The corresponding trajectory traces of Na^+ as well as O^{2-} are further depicted in Fig.8. Evidently, the Na^+ trajectory is 2-dimensional along the z-axis (or c-axis in the lattice coordinate, *viz.* parallel to the SiO_4 layer) with large displacement. In contrast, the simulated O^{2-} trajectory is represented by a group of random and unsuccessful jumps with much smaller displacement.

Another distinct feature of the Na^+ trajectories is that they are separated into modes associated with vibration at a fixed site and transport between two sites. This observation provides strong evidence that Na^+-transport occurs by discrete hops between two adjacent sites. In other words, Na ions are localized at a particular site for several oscillation periods before jumping to another site at a near distance. Similar hopping mechanism has also been

proposed for the same material [14].

3.2 Na^+ transport in the crystalline $Na_2Si_2O_5$

To investigate if the high mobility of Na^+ is a unique feature for the amorhous $Na_2Si_2O_5$, we also simulated Na^+ diffusion dynamics in a crystalline $Na_2Si_2O_5$. To do so, one Na atom is virtually removed from the lattice to create a Na vacancy, followed by Na^+ hopping via Na-vacancies. Based on the symmetry of the $Na_2Si_2O_5$ crystal structure, three distinct directions, namely, X, Y and Z, were specified for Na^+ transport; see Fig.9 (a), (c), and (e). It is worth mentioning that along the Z-direction Na^+ are transported between the two corner-shared SiO_4 layers. The corresponding energy profiles optimized for Na^+ transport are given in Fig.9 (b), (d), and (f). Along the X-direction, Fig.9 (a)-(b), one can see that the movement of Na^+ between the two nearest neighbors features an arced pathway with an energy barrier of 2.16 eV. Such a high energy barrier suggests that Na^+ is transported along the X-direction is unlikely. Along the Y-direction, Fig.9 (c)-(d), the path between the two nearest neighbors is longer and features a zigzag pathway passing through the SiO_4 tetrahedra layers. The energy barrier is as high as 2.14 eV, indicating that Na^+ movement along the Y-direction is also less favorable. The lowest energy barrier is 1.18 eV observed for movement along the Z-direction, Fig.9 (e)-(f), a two-dimensional channel formed by corner-shared SiO_4 tetrahedra, although it is probably too high for a fast Na^+ transport.

To further confirm that fast Na^+ conduction is unique for amorphous $Na_2Si_2O_5$, we also performed *ab-initio* molecular dynamics simulations on crystalline $Na_2Si_2O_5$ at 723, 773, 823, and 873K, respectively, for 8ps. The parameters of AIMD were the same as those used in the

amorphous $Na_2Si_2O_5$. The mean square displacements (MSDs) for Na, O, and Si ions simulated at these temperatures are shown in the Fig.10. It is evident that the MSDs indicate no significant Na^+ diffusion in the crystalline $Na_2Si_2O_5$ as in the amorphous counterpart at the elevated temperatures.

Overall, it is rather clear that the Na^+ transport in the amorphous $Na_2Si_2O_5$ is much faster than that in the crystalline form. One fundamental reason is that the high energy barrier for Na^+ through channels formed by corner-shared SiO_4 tetrahedra in the crystalline $Na_2Si_2O_5$ is significantly lowered by the long-range disordering in the amorphous phase $Na_2Si_2O_5$, thus increasing Na^+ conductivity.

IV. **Conclusions**

The AIMD simulations of ionic transport in the amorphous $Na_2Si_2O_5$ strongly suggest that the predominant mobile charge carrier is Na^+. The MSD of Na^+ features a linear increase with time whereas those of O^{2-} and Si^{4+} show time-independent plateaus. The RDF analysis further reveals the absence of Na-Na separation in the total g(r), implying a fast Na^+ conduction. The movement of Na^+ in the amorphous $Na_2Si_2O_5$ is a low-energy process, yielding a self-diffusivity at least two orders of magnitude higher than O^{2-} and Si^{4+}. The simulated activation energy for Na^+ agrees well with those reported in the literature for the well-known Na^+-conductor Na-β”-Al_2O_3. The calculated conductivity is found higher than the experimental data, the reason of which is related to the continuous glass-to-ceramic transition experienced during the experimental conductivity measurement, resulting in lowered

conductivity. The simulation of Na^+ transport pathways indicates that Na^+ preferentially diffuses within the layered channels formed by corner-shared SiO_4 tetrahedra in short-range ordering and long-range disordering. Similar simulation of Na^+ across a crystalline $Na_2Si_2O_5$ suggests that crystalline $Na_2Si_2O_5$ is virtually an electrical insulator with a high energy barrier. Among the three crystallographic directions simulated, the energy barrier is the lowest for the Z-direction, along the layers formed by corner-shared SiO_4 tetrahedra. Overall, the amorphous $Na_2Si_2O_5$ is a promising Na^+ conductor.

Acknowledgment

This work was funded by the Advanced Research Projects Agency-Energy (ARPA-E), U.S. Department of Energy, under Award number DE-AR0000492. Partial support from NSF (CBET-1264706) is also acknowledged.

References

1 A. J. Jacobson, *Chem. Mater.*, 2010, **22**, 660.

2 L. Malavasi, C. A. J. Fisher and M. S. Islam, *Chem. Soc. Rev.*, 2010, **39**, 4370.

3 A. Aguadero, L. Fawcett, S. Taub, R. Woolley, K. Wu, N. Xu, J. A. Kilner and S. J. Skinner, *J. Mater. Sci.*, 2012, **47**, 3925.

4 P. Singh and J. B. Goodenough, *Energy Environ. Sci.*, 2012, **5**, 9626–9631.

5 P. Singh and J. B. Goodenough, *J. Am. Chem. Soc.*, 2013, **135**, 10149–10154.

6 R. Martinez, P. Singh, J. A. Alonso and J. B. Goodenough, *J. Mater. Chem. A*, 2014, **2**, 4355–4360.

7 T. Wei, P. Singh, Y. Gong, J. B. Goodenough, Y. Huang and K. Huang, *Energy Environ. Sci.*, 2014, **7**, 1680–1684.

8 J. G. Xu, X. M. Wang, H. Fu, C. M. Brown, X. P. Jing, F. H. Liao, F. Q. Lu, X. H. Li, X. J. Kuang, and M. M. Wu, *Inorg. Chem.,* 2014, **53**, 6962.

9 R. D. Bayliss, S. N. Cook, S. Fearn, J. A. Kilner, C. Greaves, and S. J. Skinner, *Energy Environ. Sci.,* 2014, **7**, 2999.

10 R. D. Bayliss, S. N. Cook, D. O. Scanlon, S. Fearn, J. Cabana, C. Greaves, J. A. Kilner and S. J. Skinner, *J. Mater. Chem. A,* 2014, **2**, 17919.

11 I. R. Evans, J. S. O. Evan, H. G. Davies, A. R. Haworth, and M. L. Tate, *Chem. Mater.,* 2014, **26**, 5187.

12 C. Tealdi, L. Malavasi, I. Uda, C. Ferrara, V. Berbenni, and P. Mustarelli, *Chem. Commun.,* 2014, **50**, 14732.

13 S. Fernández-Palacios, L. Santos-Gómez, J. M. Compana, J. M. Porras-Vázquez, A. Cabeza, D. Marrero-López, and E. R. Losilla, *Ceram. Int.,* 2015, **41**, 6542.

14 W. Smith, G. N. Greaves, M. J. Gillan, *J. Chem. Phys.* 1995, **103** (8), 22.

15 W. Smith, G. N. Greaves, M. J. Gillan, *J. Non-Cryst. Solids*, 192 & 193 (1995) 267-271

16 W. Smith, T. R. Forester, G. N. Greaves, S. Haytera and M. J. Gillanb, *J. Mater. Chem.*, 1997, **7(2)**, 331–336.

17 P. E. Blöchl, Projector augmented-wave method. *Phys. Rev. B*, 1994, **50**, 17953-17979.

18 G. Kresse, D. Joubert, From ultrasoft pseudopotentials to the projector augmented-wave method. *Phys. Rev. B*, 1999, **59**, 1758-1775.

19 G. Kresse, J. Hafner, *Phys. Rev. B*, 1993, **47**, RC558-561.

20 G. Kresse, J. Furthmüller, *Phys. Rev. B*, 1996, **54**, 11169-11186.

21 J. P. Perdew, K. Burke, M. Ernzerhof, Generalized Gradient Approximation Made Simple. *Phys. Rev. Lett.*, 1996, **77**, 3865–3868.

22 G. Mills and H. Jónsson, *Phys. Rev. Lett.*, 1994, **72**, 1124-1127.

23 G. Mills, H. Jónsson, and G. K. Schenter, *Surf. Sci.* 1995, **324**, 305-337.

24 Michael E. Fleet, and Grant S. Henderson, *J. Solid State Chem.*, 1995, **119**, 400-404.

25 M. Misawa, D. L. Price, and K. Suzuki, *J. Non-Cryst Solids*, 1980, **37**, 85-97.

26 G. E. March, *Solid State Ionics.*, 1982, **7**, 177-198.

27 H. Mehrer, A. W. Imre and E. Tanguep-Nijokep, *J. Phys.: Condens. Matter*, 2008, **106**, 012001.

28 F. Tietz and W. Urland, *Solid State Ionics*, 1995, **78**, 35.

29 Ch. Kaps, *J. Non-Cryst Solids*, 1984, **65**, 189-192.

30 Y. Jee, X. Zhao and K. Huang, *Chem. Commun.*, DOI: 10.1039/c5cc02638e.

31 G. H. Frischat, Ionic Diffusion in Oxide Glasses (Trans. Tech., Aedermannsdorf, 1975).

32 C. Veríssimo, F. M.S. Garridol, O. L. A1ves, P. Calle, A. Martínez-Juárez, J. E. Iglesia, J. M. Rojo, *Solid State Ionics*, 1997, **100**, 127.

33 H. Arikawa, H. Nishiguchi, T. Ishihara and Y. Takita, *Solid State Ionics*, 2000, **136–137**, 31–37.

34 B. C. H. Steele, *Solid State Ionics*, 2000, **129**, 95–110.

Table 1 calculated lattice constants, structural parameters and corresponding experimental values for crystalline $Na_2Si_2O_5$ sodium disilicate considered in this work. The units of length and angle are angstrom (Å) and degree (°), respectively. O_{br} and O_{nbr} denote the bridging and nonbridging O atom, respectively

	a	b	c	$\alpha=\beta=\gamma$	Si-O_{br}	Si-O_{nbr}	Si-O-Si
Calculated (this work)	9.539	5.656	8.468	90	1.658-1.674	1.591-1.595	125.9-129.0
Experimental	9.441	5.580	8.356	90	1.633-1.656	1.571-1.580	127.0-129.3

Table 2 Diffusion coefficient (D in 10^{-6} cm^2s^{-1}) and conductivity (σ in Scm^{-1}) of Na^+

T (K)	D_{Na}	D_O	D_{Si}	σ_{Na}	σ_{exp}
573	0.94	0.12	0.04	0.051	
623	1.22	0.10	0.05	0.061	
673	1.63	0.03	0.02	0.075	0.005
723	1.89	0.09	0.04	0.081	0.008
773	2.44	0.02	0.02	0.098	0.021
823	3.42	0.05	0.02	0.129	
873	4.39	0.13	0.05	0.156	
923	5.27	0.20	0.13	0.178	
973	6.26	0.07	0.04	0.200	

Figure Captions

Fig.1 (a) The structure of $Na_2Si_2O_5$ unit cell; (b) and corresponding density of states DOS. The red, golden, and purple balls represent the O, Si, and Na ions, respectively.

Fig.2 The average free energy versus the lattice constant scale factors.

Fig.3 The structures of (a) crystalline and (b) amorphous $Na_2Si_2O_5$, and total radial distribution function of (c) crystalline and (d) amorphous $Na_2Si_2O_5$ simulated at 973 K.

Fig.4 Partial radial pair distribution function for the amorphous $Na_2Si_2O_5$ simulated at 973 K.

Fig.5 The average mean square displacement (MSD) for Na, O, and Si ions in the amorphous $Na_2Si_2O_5$ simulated in a temperature range from 573 to 973 K (in steps of 50 K) for 40 ps.

Fig.6 Arrhenius plot of Na^+ diffusivity in the amorphous $Na_2Si_2O_5$. A discontinuity at 773K is observed.

Fig.7 The Na^+ transport in the amorphous $Na_2Si_2O_5$ simulated at 873K for 40 ps. The green ball represents the Na^+ in motion.

Fig.8 The calculated ion transport trajectories in the amorphous $Na_2Si_2O_5$. (a) for Na^+ and (b) for O^{2-}. The AIMD was run at 873K for 40 ps.

Fig.9 The minimum energy transport pathways and calculated corresponding energy profiles of a single Na^+ along the X direction (a)-(b), Y direction (c)-(d), and Z direction (e)-(f). The red, golden, and purple balls represent O, Si, and Na ions, respectively. The blue balls are the moving Na^+. The pathway with the lowest energy is along the Z-direction, which is between two adjacent SiO_4 layers.

Fig.10 The averaged MSD for Na, O, and Si ions in the crystalline $Na_2Si_2O_5$ simulated in a temperature range from 723 to 873 K (in steps of 50 K) for 8ps.

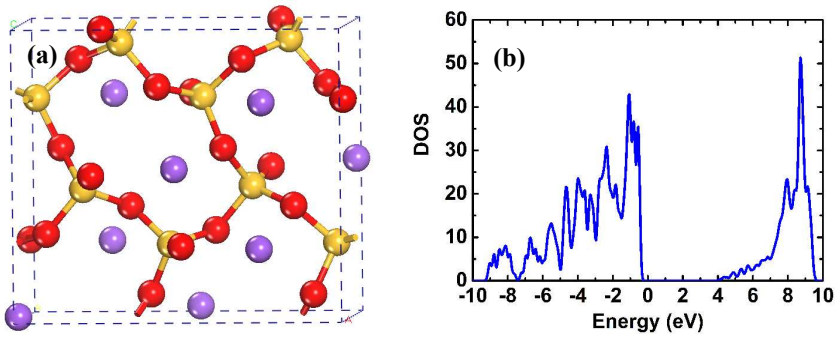

Fig. 1

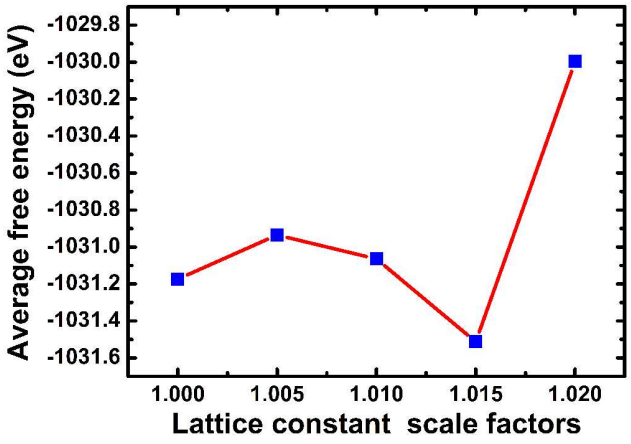

Fig. 2

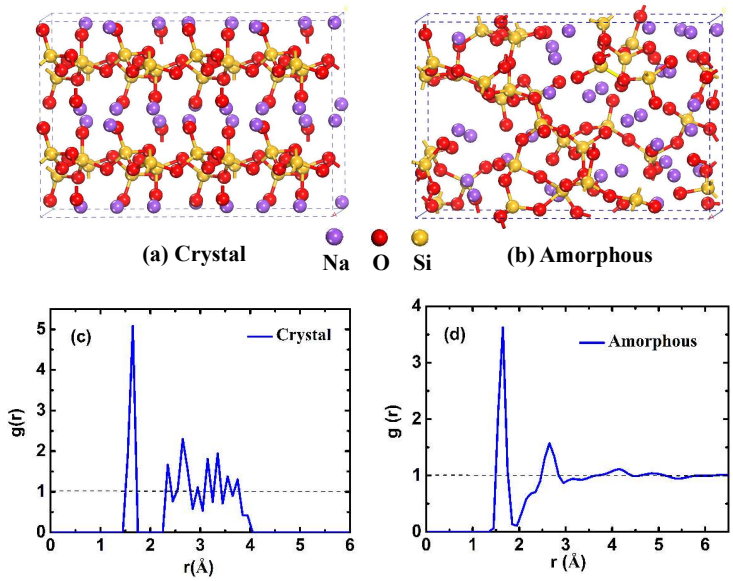

Fig.3

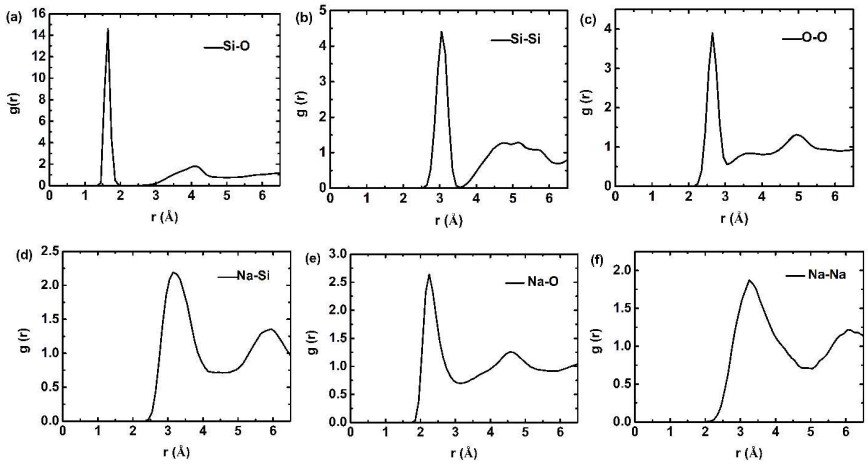

Fig.4

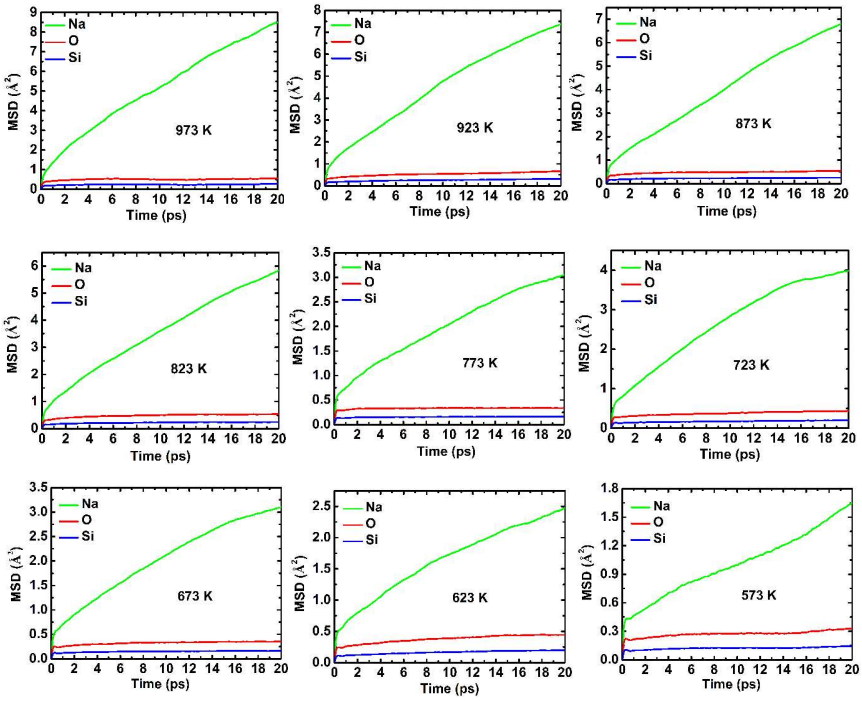

Fig.5

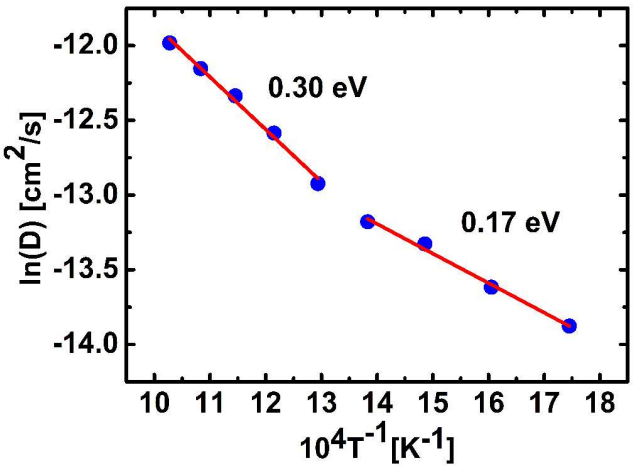

Fig.6

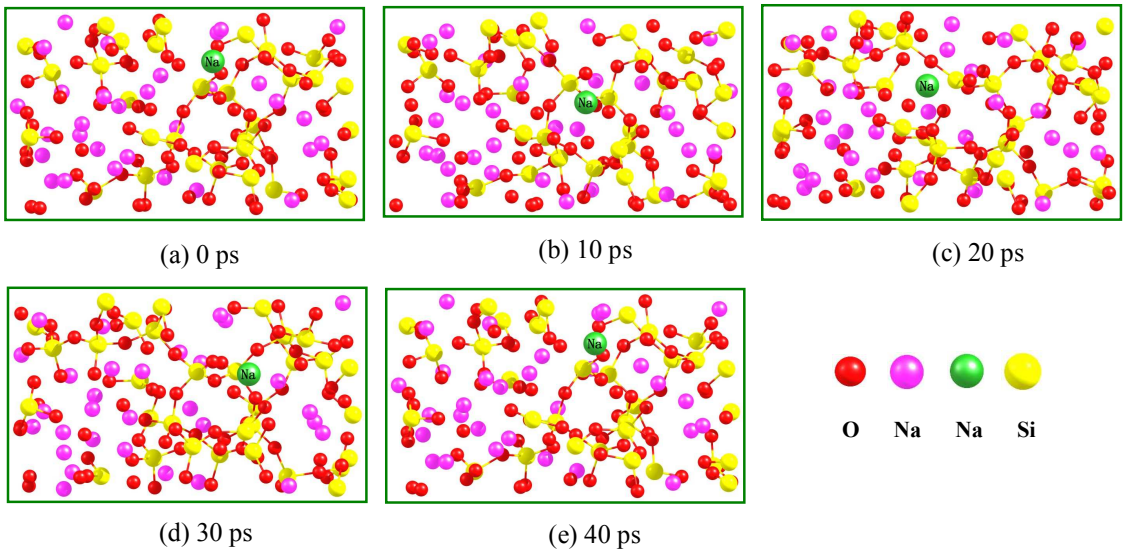

(a) 0 ps (b) 10 ps (c) 20 ps

(d) 30 ps (e) 40 ps

Fig.7

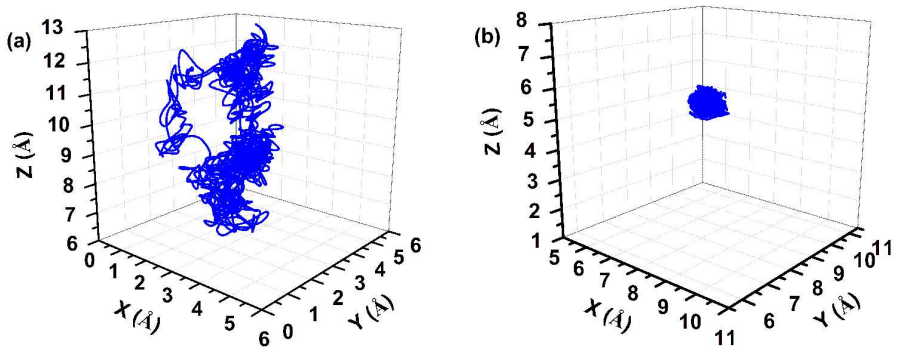

Fig.8

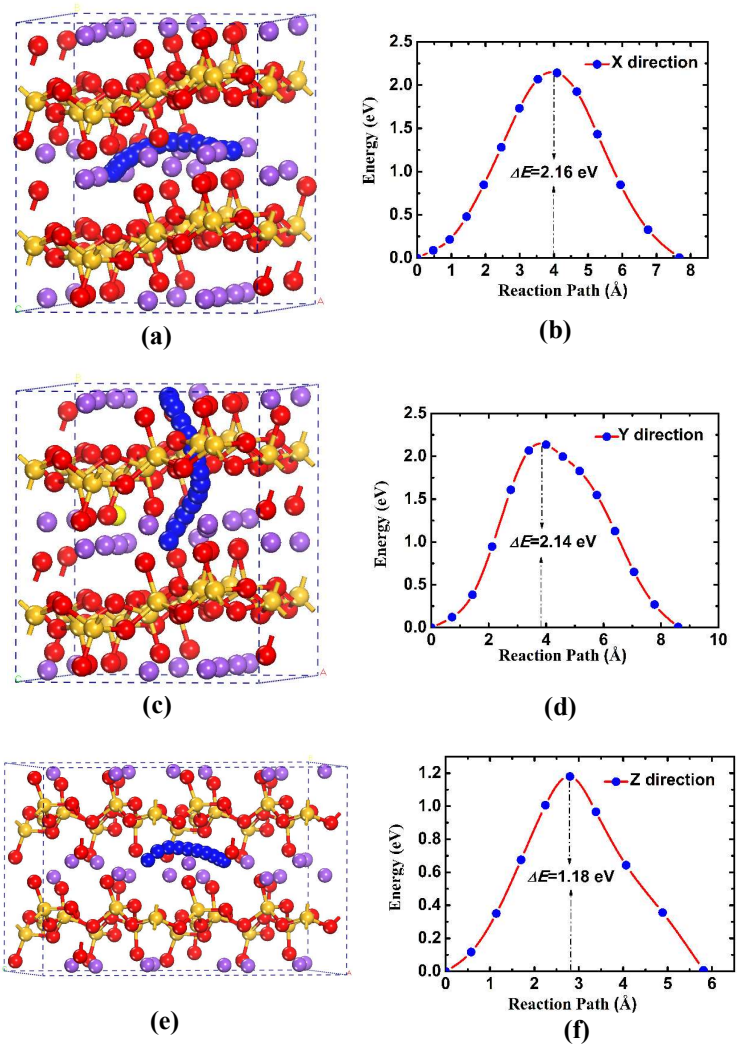

Fig.9

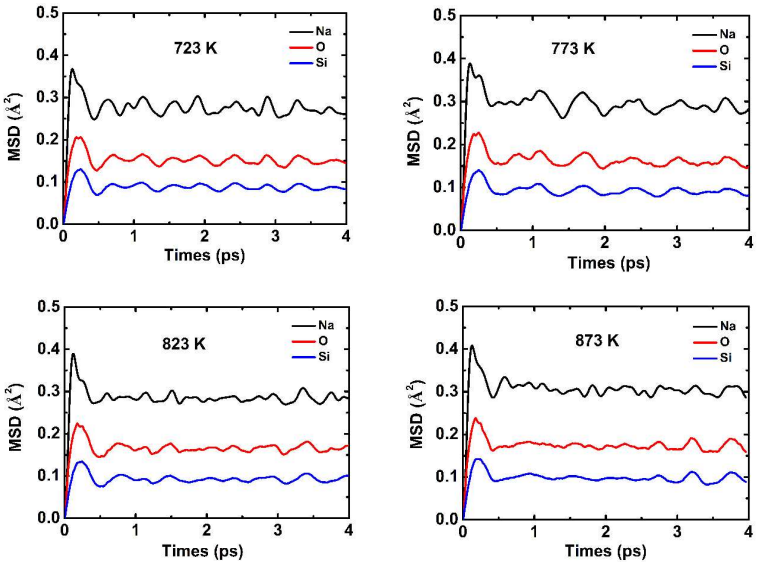

Fig. 10

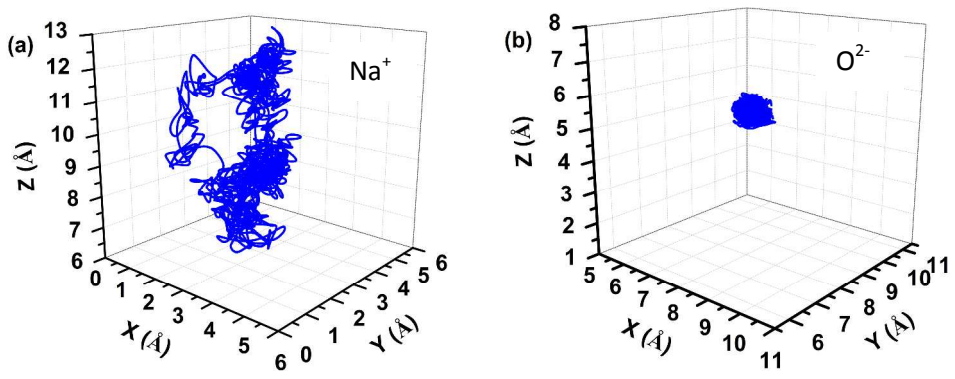

An *ab-initio* molecular dynamics simulation suggests a fast Na^+ conduction in amorphous $Na_2Si_2O_5$